Thesis for Bachelor's Degree

Physically-based simulation of falling paper motion

Seoyoung Choi

Electrical Engineering and Computer Science Concentration

Gwangju Institute of Science and Technology

2016

Physically-based simulation of falling paper motion

종이 낙하운동의

물리기반 시뮬레이션

Physically-based simulation of falling paper

Advisor: Professor Unjong Yu

by

Seoyoung Choi

Electrical Engineering and Computer Science Track

Gwangju Institute of Science and Technology

A thesis submitted to the faculty of the Gwangju Institute of Science and Technology in partial fulfillment of the requirements for the degree of Bachelor of Science in the Electrical Engineering and Computer Science Concentration.

Gwangju, Republic of Korea

2016.06.23.

Approved by

Professor Unjong Yu

Committee Chair

Physically-based simulation of falling paper

Seoyoung Choi

Accepted in partial fulfillment of the requirements for the degree of

Bachelor of Science

2016.06.23.

Committee Chair _____

Prof. Unjong Yu

Committee Member _____

Prof. Kuk-Jin Yoon

Committee Member _____

Prof. Kin Choong Yow

BS/EC Seoyoung Choi (최서영). Physically-based simulation of falling paper motion (종이 낙

20125090 하운동의 물리기반 시뮬레이션). Electrical Engineering and Computer Science Concentration. 2016. 21p. Prof. Unjong Yu.

Abstract

The dynamics of a falling paper has been a popular research topic in fluid mechanics. However, due to the complexity of the problem, the simulations are limited to simple motions or two-dimension. This paper presents a simulation method that is computationally efficient, but not limited to simple motions or two-dimension. The method modifies a two-dimensional model to integrate the effects of three-dimensional features, such as total area and aspect ratio, on a falling paper. Thus, the method simulates visually as well as physically plausible motion of a falling paper.

KEYWORDS: dynamics of a falling paper/plate, tumbling and fluttering motion, transition of falling paper/plate motion

Contents

List of Tables

List of Figures

I. Introduction

An object falling in a fluid, such as a leaf falling in the air, displays a motion that seems regular, chaotic, or even both. Explaining the transitions from one motion to another requires understanding its dynamics. When an objects falls in a fluid, vortices are formed in the vicinity of the object. The vortices result in lift and drag forces which are essential in describing the falling motion [Xie and Miyata 2013].

Due to the complexity of the dynamics and long computation time, often a falling object is restricted to a simpler form such as a thin, rigid circular disc or rectangular paper. The motion of such falling object is classified into the four motion types: tumbling motion, chaotic motion, fluttering motion, and steady fall motion. A paper is said to tumble when it exhibits periodically rotating motion. It is said to flutter when it sways from side to side periodically during the fall. Chaotic motion is a mixture of tumbling and fluttering motion. A paper is in steady fall motion if it simply falls perpendicular to the ground [Field et al. 1997]. See Fig. 1 for motion classifications.

Anderson et al. [2005] took vortices into account by using direct numerical simulations of two-dimensional Navier-Stokes equation to simulate a falling card. Also, they used thickness-to-broadside-length ratio, the dimensionless moment of inertia, and the Reynold's number to explain the transitions. While this model depicts dynamic motions, it is limited to two-dimension. On the other hand, Weißmann and Pinkall [2013] simulated three-dimensional bodies sinking underwater, using Kirchoff's equations to discount the effects of the vortices, by setting the circulation of the surrounding fluid to a constant value. Tanabe and Kaneko [1994] proposed a simple model that describes and simulates the behavior of a thin, rigid paper on two-dimensional plane without using the Navier-Stokes equation. Xie and Miyata [2013] simulated lightweight rigid bodies using precomputed trajectory database and motion synthesis.

Experimental approach has been also taken to describe the motion of a falling object. Field et al. [1997] conducted experiments of steel and lead discs falling through water-glycerol mixtures and distinguishes the transitions of the motion by Reynold's number and dimensionless moment of inertia. Kanso et al. [2014] experimented coins falling in water and focuses on the differences in the landing position due to the transitions of the motion. This experiment was also conducted by changing the variables that reflect the

effects of Reynold's number and dimensionless moment of inertia. Mahadevan et al. [1999] experimented with a flat, thin card tumbling through the air to show the relationship between the tumbling frequency and the width, thickness of the card. Wang et al. [2013] studies the influence of aspect ratio on a tumbling plate such as its descent angle, rotating speed, descent velocities, lift and drag coefficients, and fluctuations in tumbling motion. However, the experiments are limited to tumbling objects [Mahadevan et al. 1999; Wang et. al 2013].

In this paper, we propose a method that simulates the motion of a paper falling in still air, in three-dimension, with minimal computation time. The method is mathematically based on the physical model which assumes two-dimensional case, thus enabling rapid computation [Tanabe and Kaneko 1994]. Also, the method uses heuristics based on the experimental results to simulate three-dimensional features such as aspect ratio and total area of the paper [Kanso et al. 2014; Wang et al. 2013]. Therefore, the simulations based on this method are computationally efficient as well as physically plausible for thin, rigid, and rectangular objects such as a small piece of paper or a leaf.

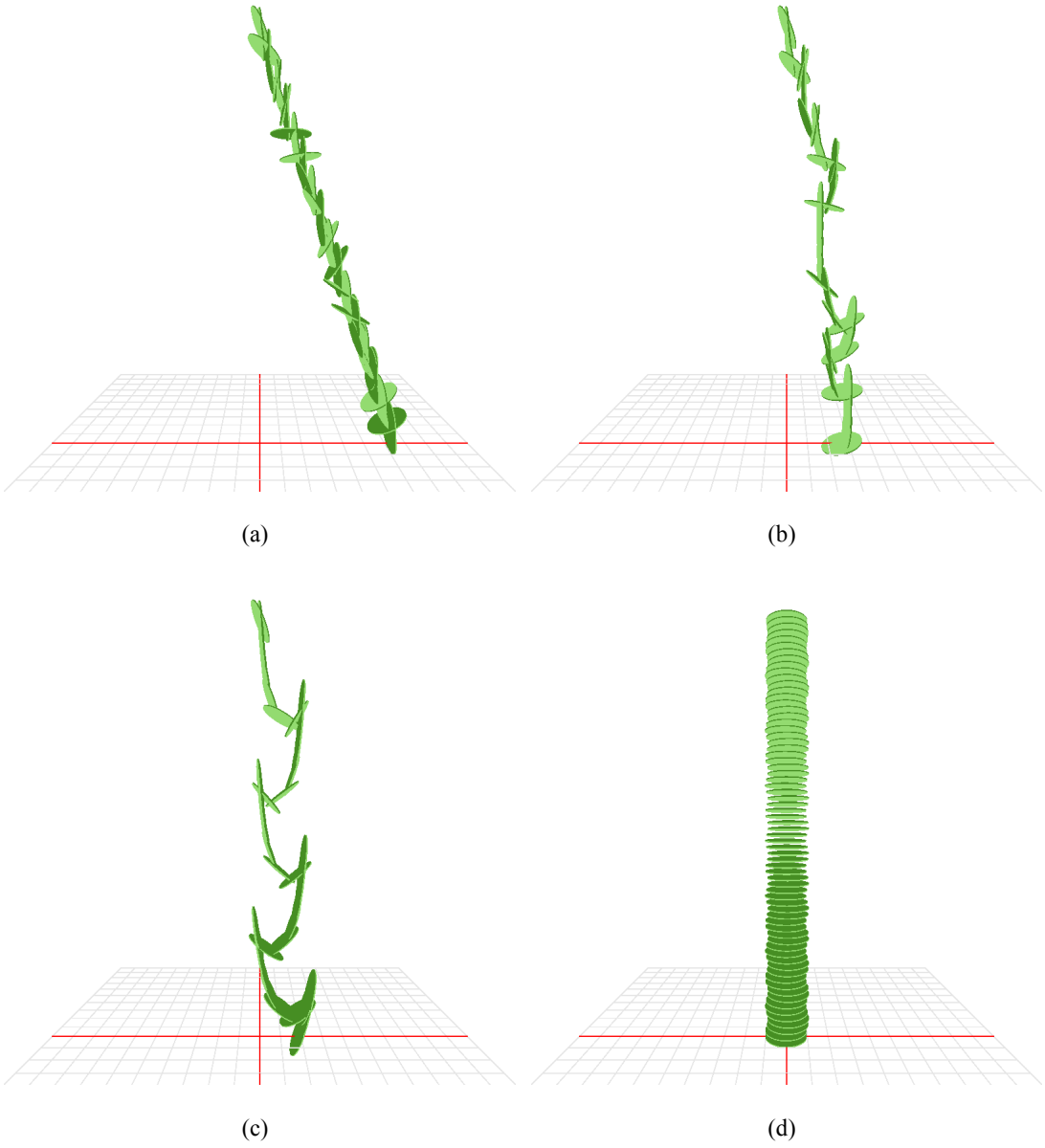

Fig. 1 Four types of falling motion. Front side of the disc is colored light green, back side dark green. (a) Tumbling motion (b) Chaotic motion (c) Fluttering motion (d) Steady fall motion

II. Mathematical Model

2.1. Ordinary Differential Equation (ODE)

The falling paper is assumed to be flat and rigid with negligible thickness. Eq. (1) is a set of ODEs that describe the motion of a falling paper in two-dimension [Tanabe and Kaneko 1994]. Eq. (1a) and Eq. (1b) describe translational motion. Eq. (1c) and Eq. (1d) describe rotational motion of the falling paper. Refer to Table. 1 for notations of variables used in Eq. (1) and Fig. 2 for visual implication of the variables.

$$\dot{u} = -(k_\perp \sin^2\theta + k_\parallel \cos^2\theta)u + (k_\perp - k_\parallel)\sin\theta\cos\theta\, v \mp \pi\rho V^2 \cos(\alpha + \theta)\cos\alpha \tag{1a}$$

$$\dot{v} = -(k_\perp \cos^2\theta + k_\parallel \sin^2\theta)v + (k_\perp - k_\parallel)\sin\theta\cos\theta\, u \pm \pi\rho V^2 \cos(\alpha + \theta)\sin\alpha - g \tag{1b}$$

$$\dot{\omega} = -k_\perp \omega - (3\pi\rho V^2 / l)\cos(\alpha + \theta)\sin(\alpha + \theta) \tag{1c}$$

$$\dot{\theta} = \omega \tag{1d}$$

2.2. Total Area and Aspect Ratio

The width of the paper, w was introduced in this paper, to consider the effects of aspect ratio and the total area of the paper on its motion. Though w is not in Eq. (1), it is implicitly included by the relative density, ρ defined as Eq. (2).

$$\rho = \frac{\rho_f}{\rho_p} = \frac{\rho_f}{m_p / l} = \rho_f \frac{l}{m_p} \tag{2}$$

w has a dimension of m, which means the dimension of the paper has changed from m to m^2 in contrast to the original model [Tanabe and Kaneko 1994]. Depending on the objective of the simulation, the width may or may not change the definition of ρ in Eq. (1). If the objective is to simulate the motion of a falling paper with respect to the total area, then Eq. (2) is used as the definition. If the objective is to simulate the effects of the aspect ratio of a falling paper, then the definition needs to be modified.

If the paper is assumed to have uniform area density, then larger total area means larger mass. To simulate the effects of increasing the total area of the paper by increasing its length, l, the mass of the paper, m_p should be proportional to l. Thus Eq. (2) can be rewritten as Eq. (3) whereas k_1 is some positive constant.

$$\rho = \rho_f \frac{k_1 \cdot l}{k_1 \cdot m_p} = \rho_f \frac{l}{m_p} \tag{3}$$

Since Eq. (2) and Eq. (3) are equivalent, Eq. (2) is used as the definition of ρ in Eq. (1).

On the other hand, to observe the effects of changing the aspect ratio while the total area is conserved, m_p should be conserved. This is because we are assuming the paper has uniform area density. Thus Eq. (2) can be rewritten as Eq. (4) whereas k_2 is some positive constant.

$$\rho = \rho_f \frac{l}{k_2} = \frac{\rho_f}{k_2} \cdot l \tag{4}$$

This implies that when ρ_f is set to be constant, then ρ is proportional to the l by the reciprocal of k_2. In this case, Eq. (5) is used instead of Eq. (1). Assume that k_2 is 1 without loss of generality.

$$\dot{u} = -(k_\perp \sin^2\theta + k_\parallel \cos^2\theta)u + (k_\perp - k_\parallel)\sin\theta\cos\theta\, v \mp \pi l V^2 \cos(\alpha + \theta)\cos\alpha \tag{5a}$$

$$\dot{v} = -(k_\perp \cos^2\theta + k_\parallel \sin^2\theta)v + (k_\perp - k_\parallel)\sin\theta\cos\theta\, u \pm \pi l V^2 \cos(\alpha + \theta)\sin\alpha - g \tag{5b}$$

$$\dot{\omega} = -k_\perp \omega - 3\pi V^2 \cos(\alpha + \theta)\sin(\alpha + \theta) \tag{5c}$$

$$\dot{\theta} = \omega \tag{5d}$$

2.3. Expansion from Line to Plane

In Eq. (1), the paper is represented as a line not a plane. In the three-dimensional case where the paper is now a thin plate, lift force expression is the same as for the two-dimensional case, but rotational induced drag is dependent on the aspect ratio. Furthermore, decreasing the aspect ratio increases translational induced drag. This results in dissipative torque, which in turn, reduces the average angular velocity [Wang et al. 2013]. Therefore, a reasonable variable which increases along with the total area or decreases with the aspect ratio should be added in the dissipative torque term. For convenience, l was added in the term to represent such effect. Thus Eq. (1c) and Eq. (5c) are modified.

In the case where l changes the total area proportionately, Eq. (6) is used.

$$\dot{u} = -(k_\perp \sin^2\theta + k_\parallel \cos^2\theta)u + (k_\perp - k_\parallel)\sin\theta\cos\theta\, v \mp \pi\rho V^2 \cos(\alpha + \theta)\cos\alpha \tag{6a}$$

$$\dot{v} = -(k_\perp \cos^2\theta + k_\parallel \sin^2\theta)v + (k_\perp - k_\parallel)\sin\theta\cos\theta\, u \pm \pi\rho V^2 \cos(\alpha + \theta)\sin\alpha - g \tag{6b}$$

$$\dot{\omega} = -k_\perp \omega l - (3\pi\rho V^2 / l)\cos(\alpha + \theta)\sin(\alpha + \theta) \tag{6c}$$

$$\dot{\theta} = \omega \tag{6d}$$

In the case where the total area is conserved while the aspect ratio is changed, Eq. (7) is used.

$$\dot{u} = -(k_\perp \sin^2\theta + k_\parallel \cos^2\theta)u + (k_\perp - k_\parallel)\sin\theta\cos\theta\, v \mp \pi l V^2 \cos(\alpha + \theta)\cos\alpha \tag{7a}$$

$$\dot{v} = -(k_\perp \cos^2\theta + k_\parallel \sin^2\theta)v + (k_\perp - k_\parallel)\sin\theta\cos\theta\, u \pm \pi l V^2 \cos(\alpha + \theta)\sin\alpha - g \tag{7b}$$

$$\dot{\omega} = -k_\perp \omega l - 3\pi V^2 \cos(\alpha + \theta)\sin(\alpha + \theta) \tag{7c}$$

$$\dot{\theta} = \omega \tag{7d}$$

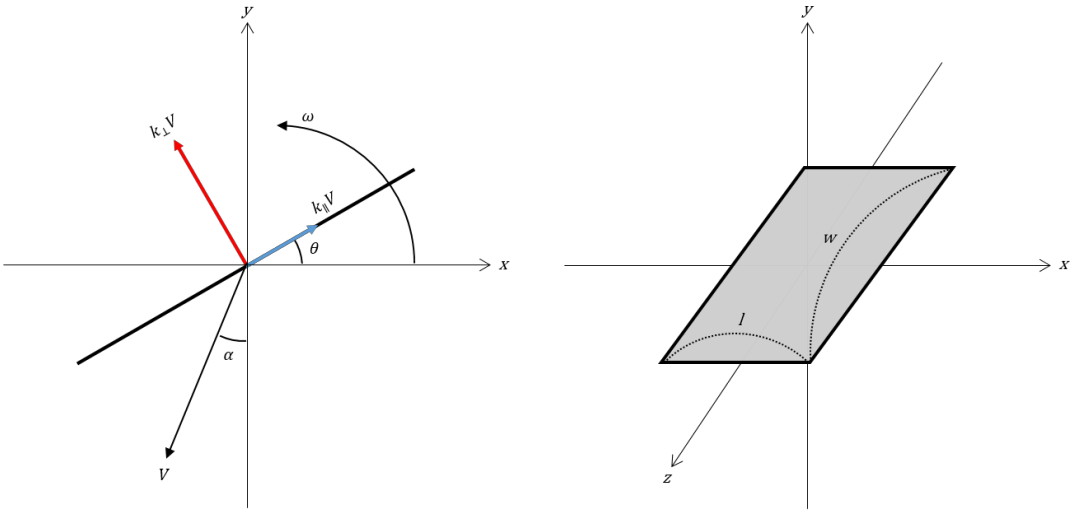

(a) (b)

Fig. 2 Visual implication of variables.
(a) Two-dimension: the red and blue arrows indicate the friction forces working on the paper.
(b) Three-dimension: the total area is determined by l and w.

Table. 1 Notations and initial values of variables

Variable	Description	Initial Value
(x, y)	Position of the center of mass of the paper	(0 m, 100 m)
(u, v)	Velocity of the center of mass of the paper	(10^{-5} m/s, 10^{-5} m/s)
θ	Angle of the paper parallel to the ground	−60 °
ω	Angular velocity (counterclockwise positive)	−10.1 rad/s
α	Angle of the direction of the fall	-
V	Magnitude of the velocity	-
$k_{\perp}$	Coefficient of the friction perpendicular to the paper	20 m^{-1} s^{-1}
$k_{\parallel}$	Coefficient of the friction parallel to the paper	0.2 m^{-1} s^{-1}
l	Length of the paper	0.1 m
w	Width of the paper	1 m
m_p	Mass of the paper	-
ρ_p	Density of the paper	-
ρ_f	Density of the fluid	1 kg/m
ρ	Relative density (ρ_f / ρ_p)	0.1
g	Gravitational acceleration	9.807 m/s^2

III. Experimental Methods

3.1. Implementation

The code was written in C++ using Visual Studio 2013 Professional. OpenGL was used as graphics library. The simulation was run on Intel® Core™ i5-4690 processor.

The simulator's virtual space where the paper falls is a cubic room of 100 m × 100 m × 100 m. The y-axis and the x-axis represent vertical and horizontal directions, respectively. The z-axis represents the depth and in this paper, the width of the paper (Fig. 4(b)).

The simulator has two projection modes, perspective and orthogonal. The paper can be rendered as a dot located at its center of mass, as an object of given shape with front and back sides, or both. In the simulation mode, the trajectory of the paper can be seen in real-time. Otherwise, the trajectory is shown as precomputed. Refer to Fig. 3 for view modes.

The position and the angle of the paper was calculated every 0.01 s using the Euler method to solve the ODEs. Double precision was used in the calculation. The computation time was measured in CPU clock seconds. The paper was rendered every 0.05 s in the real-time simulation. Refer to Table. 1 for initial values used in the computation.

3.2. Simulation

In the first simulation, the value of $k_{\perp}$ was changed while the frequency, the ratio of $k_{\perp}$ to $k_{\parallel}$ was set to be constant. Eq. (1) was used and the result was compared to that of the original work [Tanabe and Kaneko 1997]. In the second simulation, l was varied to change the total area and Eq. (6) was used. In the final simulation, l was varied to change the aspect ratio, using Eq. (7). In both simulations, the effects of varying l on the transitions of the falling motion were observed and compared to that of using Eq. (1). In all three simulations, the falling motion were classified as tumbling, chaotic, fluttering, or steady fall motion.

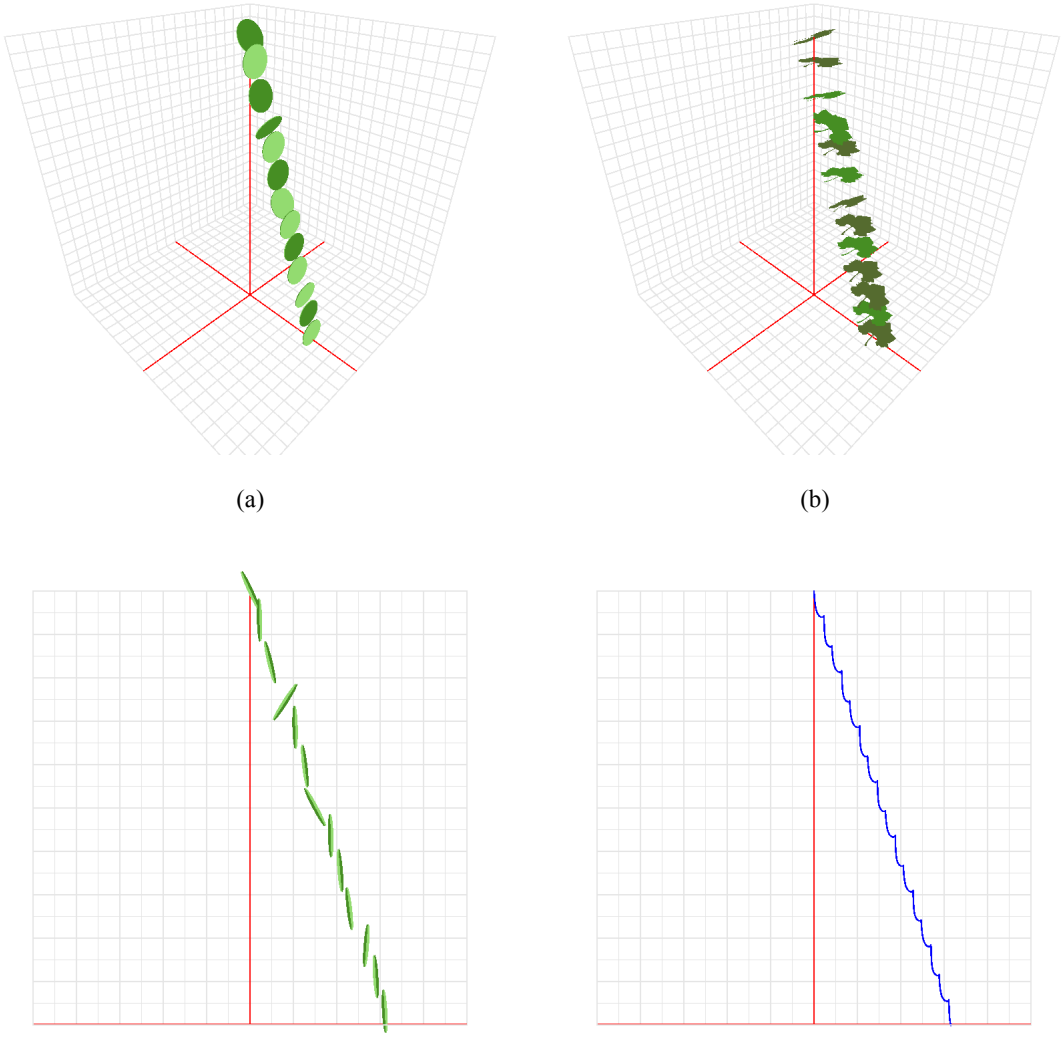

Fig. 3 Various combinations of implemented simulation modes.
Perspective projection (a) Disc simulated in real-time (b) Leaf simulated in real-time
Orthogonal projection (c) Disc simulated in real-time (d) Precomputed center of mass trajectory

IV. Result and Analysis

4.1. Frequency and Falling Motion

The simulation was run using Eq. (1), ρ was set to 0.1, and l was set to 1.0 m. The frequency was set to 100.0 since higher frequency makes it easier to distinguish the falling motions according to Tanabe and Kaneko [1994]. The values of $k_\perp$ were chosen based on their phase diagram (Fig. 4). The paper was drawn every $[t_d] \cdot 0.01$ s whereas $[t_d]$ is the Gaussian of descending time, t_d. The shape of the falling paper was shown as a disc of front and back sides with some thickness and scaled five times for better visibility.

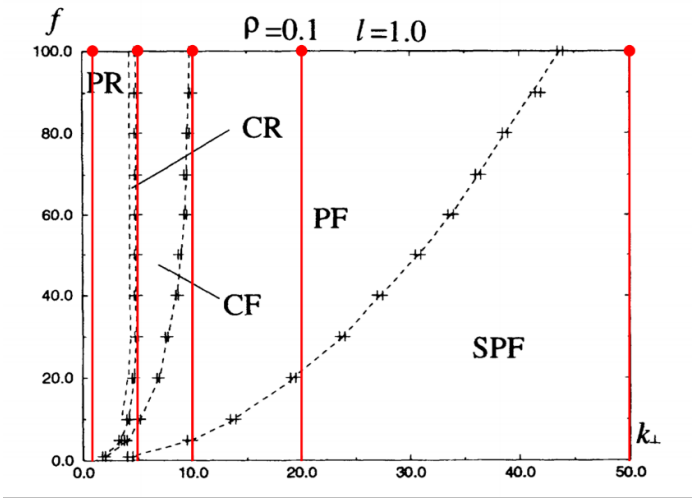

Fig. 4 Phase diagram of falling motion (Tanabe and Kaneko 1994). The phase diagram is divided into five regions: periodic rotation (PR), chaotic rotation (CR), chaotic fluttering (CF), periodic fluttering (PF), and simple perpendicular fall (SPF).

As $k_\perp$ is increased, the falling motion changes from tumbling to chaotic to fluttering motion as is apparent in Fig. 5(a), (b), and (c). However, the motion in Fig. 5(e) does not resemble a steady fall motion. This is due to the large angle of attack in the initial state of the fall. This phenomena can be seen in everyday life when a paper held almost vertically to the ground is let loose, it slices through the air rapidly. Thus, when the initial values of θ and ω were decreased, the paper exhibits steady fall motion as in Fig. 5(f). Overall, the result closely matches that of the original work.

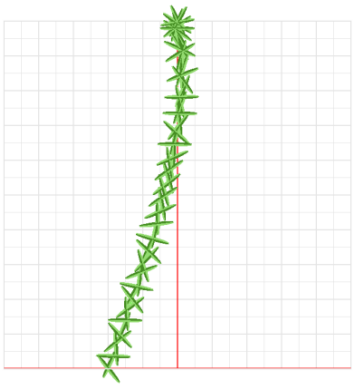

(a) $k_{\perp} = 1.0$

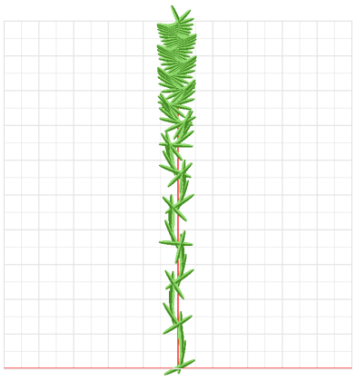

(b) $k_{\perp} = 5.0$

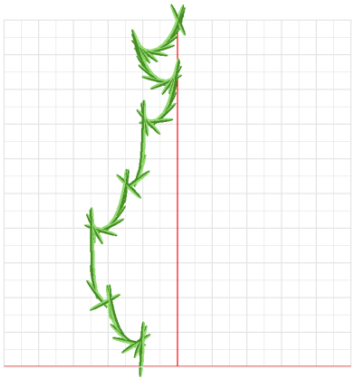

(c) $k_{\perp} = 10.0$

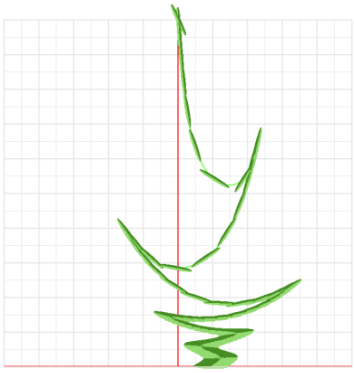

(d) $k_{\perp} = 20.0$

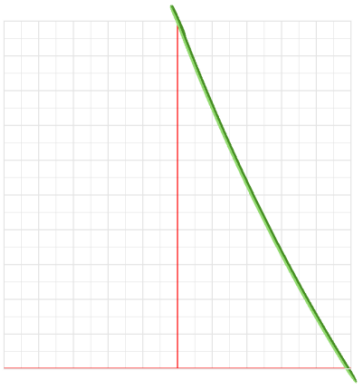

(e) $k_{\perp} = 50.0$

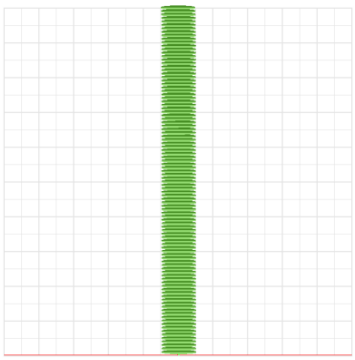

(f) $k_{\perp} = 50.0$, $\theta = -0.01$ °, $\omega = -0.01$ rad/s

Fig. 5 Transitions in the falling motion with respect to $k_{\perp}$. (a) Tumbling motion (b) Chaotic motion closer to tumbling motion (c) Chaotic motion closer to fluttering motion (d) Fluttering motion (e) Rapid drop to the sideways (f) Steady fall motion

4.2. Total Area and Falling Motion

The simulation was run using Eq. (1) or Eq. (6). Refer to Table. 1 for initial values. Only the value of l was changed explicitly. The paper was drawn every $[t_d] \cdot 0.01$ s whereas $[t_d]$ is the Gaussian of descending time, t_d. The shape of the falling paper was shown as a rectangular plate of front and back sides with some thickness and scaled five times for better visibility.

A falling paper simulated by Eq. (6) generally had greater descending time, t_{d1} than that by Eq. (1), denoted as t_{d6}. See Table. 2 for the comparison of descending time. This indicates a falling paper that actually takes area into account falls more slowly, which is indeed a desired outcome.

The visual result of using Eq. (1) and Eq. (6) are comparatively shown in Fig. 6, Fig. 7, and Fig. 8. For both simulations, when l was increased to enlarge the total area, the falling motion changed from tumbling to chaotic to fluttering. The difference in the simulations comes from the addition of l from Eq. 1(c) to Eq. 6(c). Since l was 0.1 m initially, the dissipative torque term in Eq. 6(c) is trivially smaller than that of Eq. 1(c). Thus the paper in Fig. 6(b) travels more distance before landing than that of Fig. 6(a). Also, the paper simulated using Eq. (6) generally has smaller amplitude of swings and dips when fluttering, due to the dissipative torque term. This is most apparent in Fig. 7 and Fig. 8.

Table. 2 Quantitative result using Eq. (1) and Eq. (6)

l (m)	t_{d1} (s)	t_{d6} (s)
0.1	24.40	78.07
0.2	21.21	63.52
0.3	18.34	85.43
0.4	18.25	48.26
0.5	19.87	84.25
0.6	49.43	95.39
Δt_d (s)	25.25	78.82

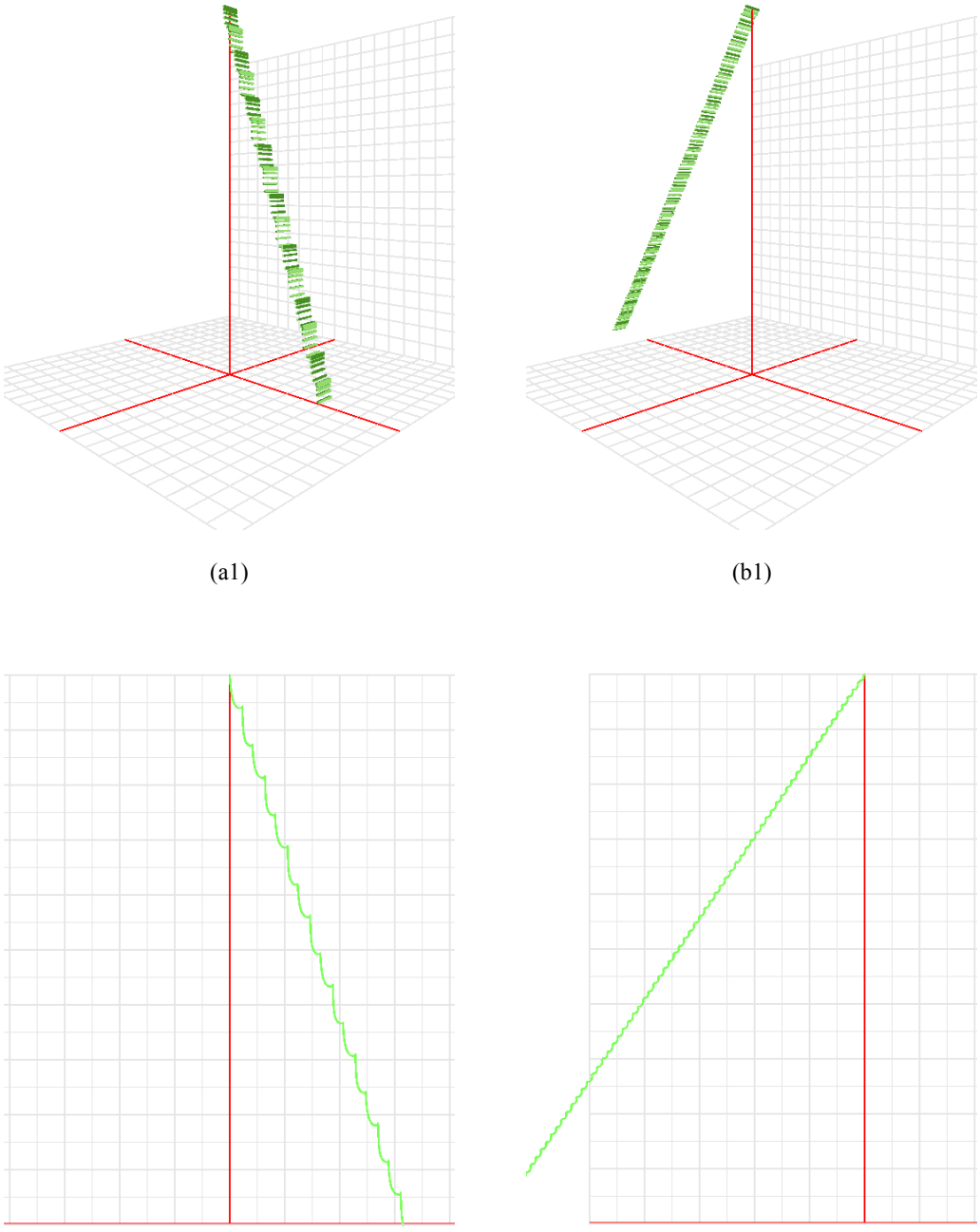

(a1) (b1)

(a2) (b2)

l = 0.1 m. Tumbling motion.

Fig. 6 Total area simulation. (a1) and (a2) uses Eq. (1) while (b1) and (b2) uses Eq. (6) for simulation.

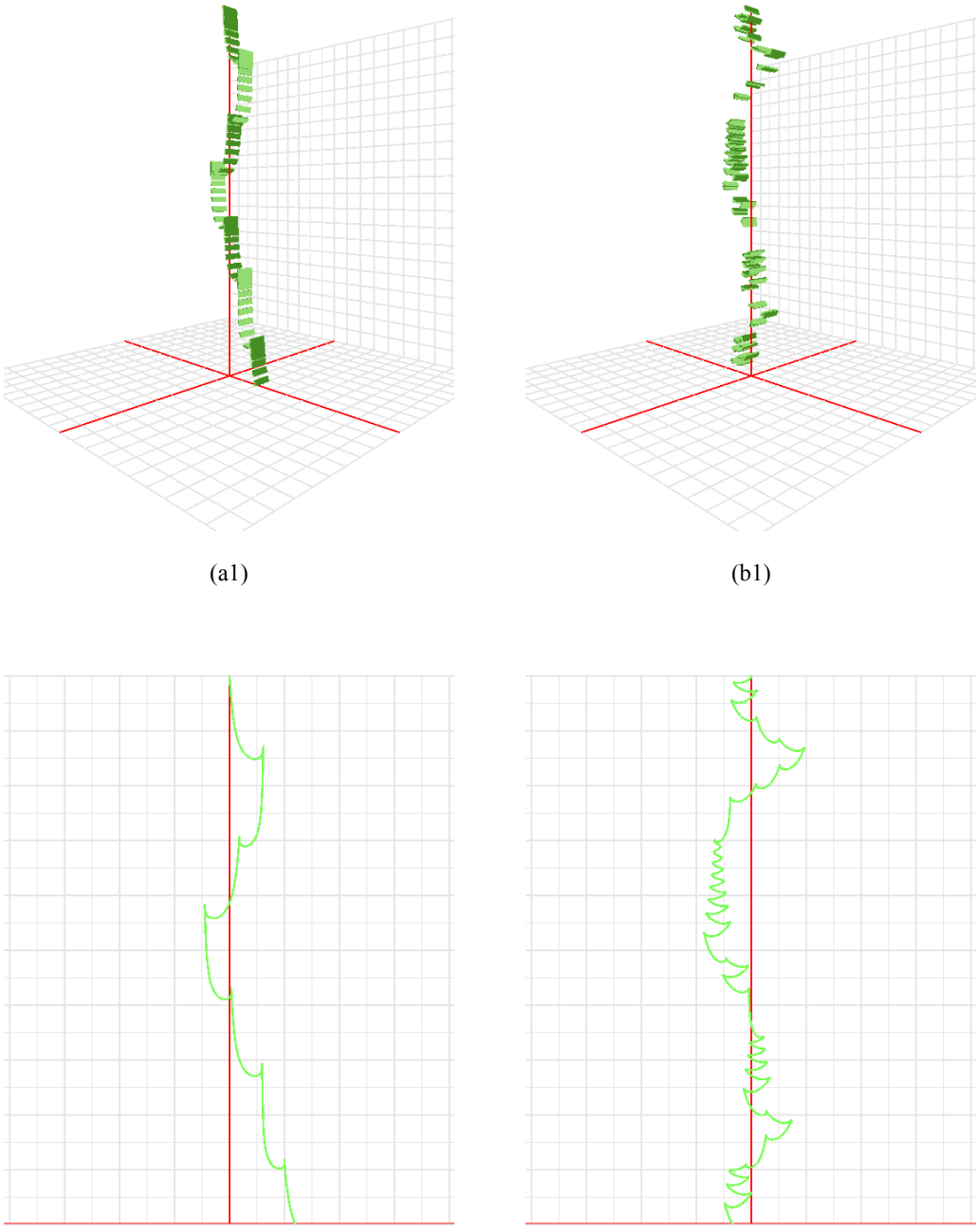

(a1) (b1)

(a2) (b2)

l = 0.3 m. Chaotic motion.

Fig. 7 Total area simulation. (a1) and (a2) uses Eq. (1) while (b1) and (b2) uses Eq. (6) for simulation.

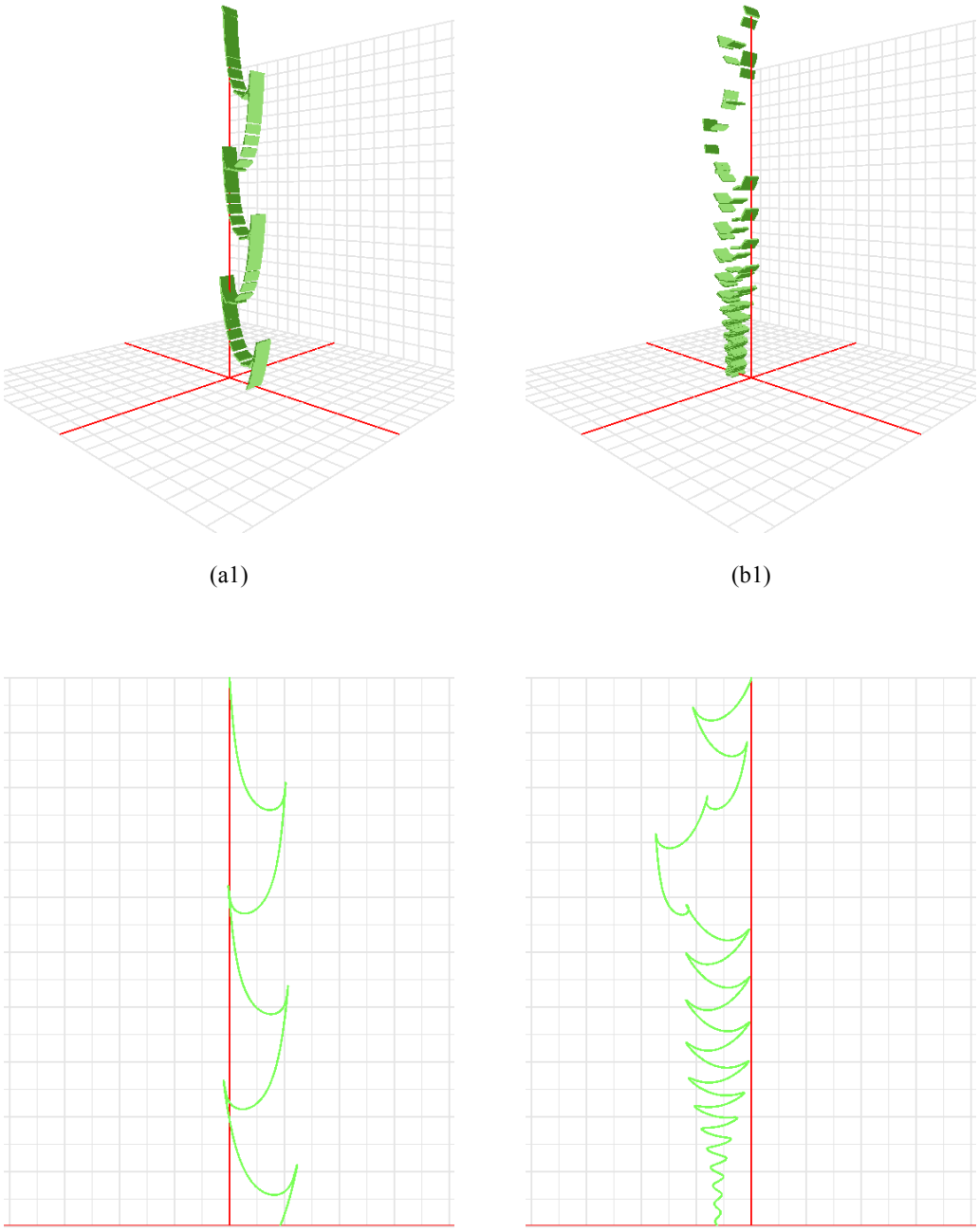

l = 0.5 m. Fluttering motion.

Fig. 8 Total area simulation. (a1) and (a2) uses Eq. (1) while (b1) and (b2) uses Eq. (6) for simulation.

4.3. Aspect Ratio and Falling Motion

The simulation was run using Eq. (1) or Eq. (7). Initially, the value of w was set to 0.2 m to make the initial aspect ratio of 2:1. Also, the initial x-position was changed to fit within the camera view. Otherwise, refer to Table. 1 for initial values. Only the value of l was changed explicitly. The paper was drawn every $[t_d] \cdot 0.01$ s whereas $[t_d]$ is the Gaussian of descending time, t_d. If there were more than one paper being simulated at once, the papers were drawn every $min([t_d]) \cdot 0.01$ s. The shape of the falling paper was shown as a rectangular plate of front and back sides with some thickness and scaled fifty times for better visibility.

The result of using Eq. (1) and Eq. (7) are comparatively shown in Fig. 9 and Table. 3. In Fig. 9, the green plate has the aspect ratio of 2:1 while the blue plate has the aspect ratio of 8:1. Both simulations show tumbling motion of the falling papers. However, the result of the simulation using Eq. (1) apparent in Fig. 9(a) and Table. 3 is incorrect. The increment of the length implies decrement in aspect ratio. Smaller aspect ratio decreases t_d, number of turns(n), landing distance(Δx), and increases descent angle [Wang et al. 2013], but the landing distance of the blue plate, which has larger aspect ratio, is less than that of the green plate. This is because in Eq. (1), as l was increased, the total area and thus m_p were increased along with it.

Table. 3 Quantitative result using Eq. (1) and Eq. (7)

l (m)	t_{d1} (s)	n_1	Δx_1 (m)	t_{d7} (s)	n_7	Δx_7 (m)
0.05	27.77	25	78.6427	104.31	225	25.9988
0.1	24.4	15	81.5816	78.07	145	17.4954

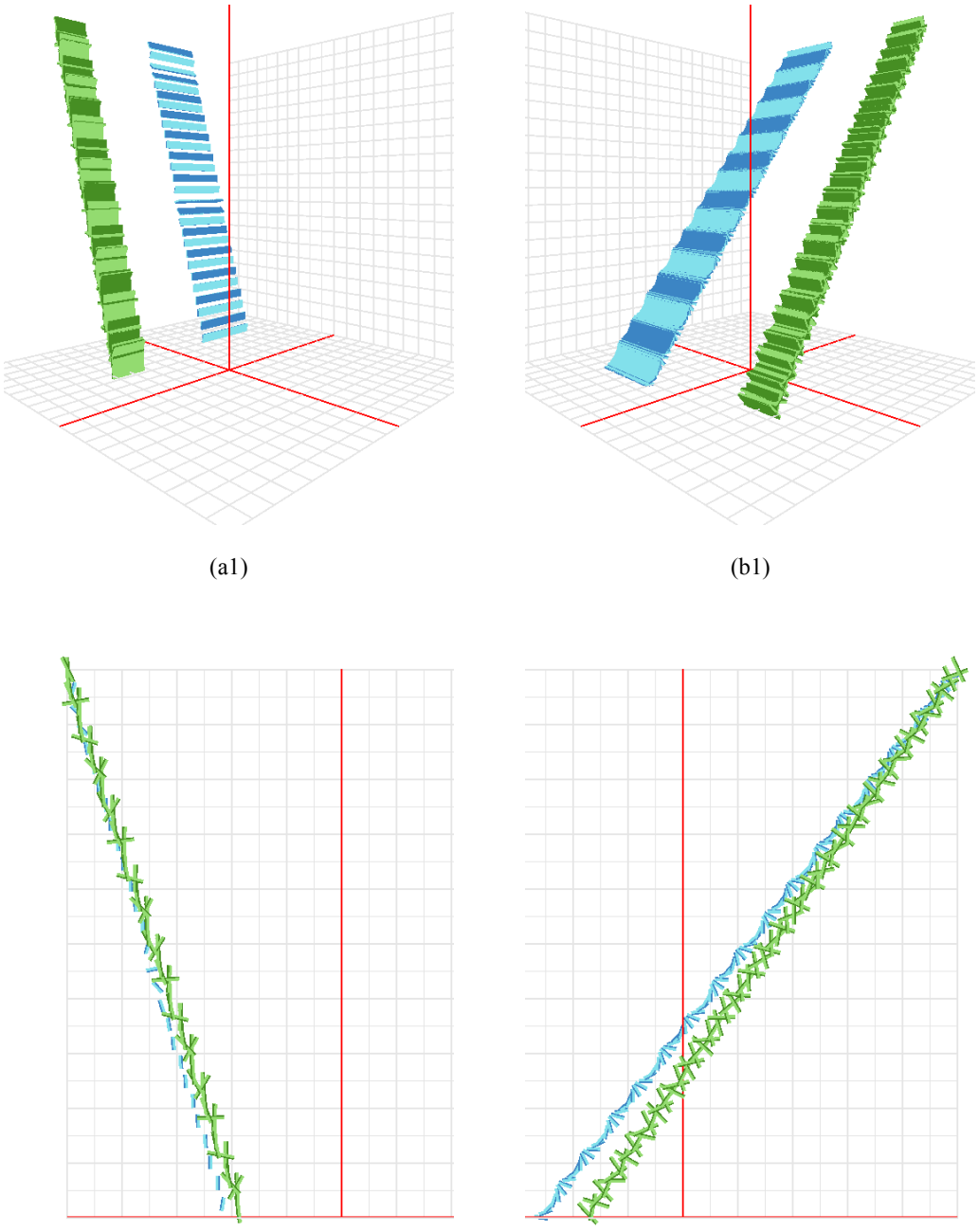

Fig. 9 Aspect ratio simulation. (a1) and (a2) uses Eq. (1) while (b1) and (b2) uses Eq. (7) for simulation.

The result of decreasing aspect ratio only using Eq. (7) is shown in Fig. 10. This time, the shape of the falling paper was scaled ten times for better visibility. When aspect ratio was decreased, the motion of the paper changed from tumbling to chaotic to fluttering. Other variables being the same, larger l means smaller thickness-to-length ratio. When decreasing thickness-to-length ratio and consequently the dimensionless moment of inertia, the motion changes from tumbling to fluttering [Anderson et al. 2005]. Therefore, it can be deduced from their research that when the aspect ratio is decreased, the motion changes from tumbling to fluttering. The simulation result matches the deduction.

In reality, however, the motion shown in Fig. 10(c) rarely happens. An actual paper with such small aspect ratio would flutter for a moment and then start tumbling. This discrepancy comes from the dimension difference between the mathematical model and the real world. If the mathematical model were to be extended to resemble the motion in the real world, variables describing translational and rotational motions in the z-axis would have to be adopted.

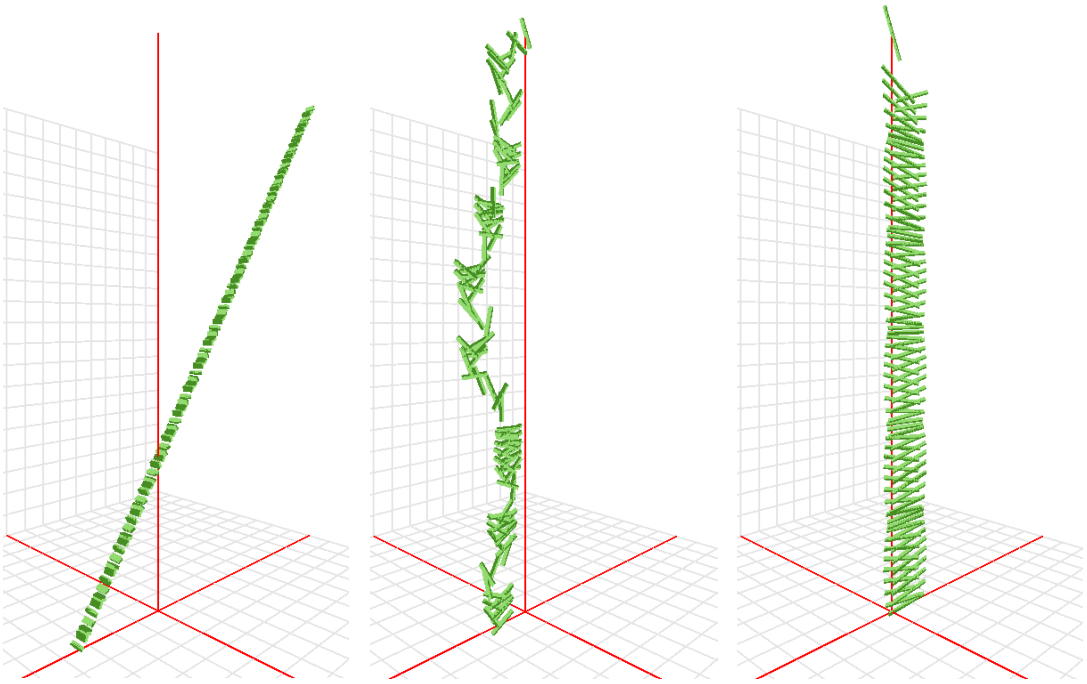

(a) 2:1 (b) 2:25 (c) 2:81

Fig. 10 Aspect ratio simulation. (a) Tumbling motion (b) Chaotic motion (c) Fluttering motion

V. Conclusion

The proposed method considers the effects of total area and aspect ratio on the falling motion of a thin, rigid, and rectangular paper. When the total area was increased, the paper fell more slowly in a less turbulent manner. When the aspect ratio was decreased, the paper changed its motion from tumbling to chaotic to fluttering. Thus the method, which is based on the original model proposed by Tanabe and Kaneko [1994], extends to simulating the falling motion of a three-dimensional paper. Combined with computational efficiency of the original model and visual as well as mathematical plausibility, our method can be further applied to simulating multiple objects at once, such as falling autumn leaves, flying cards, or paper flakes of a confetti.

VI. References

ANDERSEN, A., PESAVENTO, U., AND WANG, Z. J. 2005. Analysis of transitions between fluttering, tumbling and steady descent of falling cards. *Journal of Fluid Mechanics* 541, 91-104.

FIELD, S. B., KLAUS, M., MOORE, M. G., AND NORI, F. 1997. Chaotic dynamics of falling disks. *Nature* 388, 6639, 252-254.

KANSO, E., HEISINGER, L. AND NEWTON, P. 2014. Coins falling in water. *Journal of Fluid Mechanics* 742, 243-253.

MAHADEVAN, L., RYU, W. S., AND SAMUEL, A. D. 1999. Tumbling cards. *Physics of Fluids* 11, 1, 1-3.

TANABE, Y. AND KANEKO, K. 1994. Behavior of a Falling Paper. *Physical Review Letters* 73, 10, 1372-1375.

WANG, W. B., HU, R. F., XU, S. J., AND WU, Z. N. 2013. Influence of aspect ratio on tumbling plates. *Journal of Fluid Mechanics* 733, 650-679.

WEIßMANN, S. AND PINKALL, U. 2012. Underwater rigid body dynamics. *ACM Transactions on Graphics* 31, 4, 1-7.

XIE, H. AND MIYATA, K. 2013. Real-time simulation of lightweight rigid bodies. *The Visual Computer 30*, 1, 81-92.

VII. Acknowledgement

Linear thanks to fried chickens and exponential thanks to my advisor, Prof. Unjong Yu, for supporting me throughout the four years. Special thanks to Prof. Kin Choong Yow and Prof. Kuk-Jin Yoon for being the referees of my thesis.

And thank you curry much for the intricate leaf model, Dr. Seungho Baek.